Research in Astronomy and Astrophysics, 23:115014 (7pp), 2023 November https://doi.org/10.1088/1674-4527/acf6f6

Study on the X-Ray Re-brightening Signature of GRB 220117A

Li-Tao Zhao
School of Mathematics and Science, Hebei GEO University, Shijiazhuang 050016, China; zhaolt@mail.bnu.edu.cn
Received 2023 July 24; revised 2023 August 25; accepted 2023 September 4; published 2023 October 9

Abstract

The Swift/XRT detected the X-ray afterglow of long burst GRB 220117A, which began to rebrighten 300 s after triggering and followed a single power-law decay segment after thousands of seconds of the orbital observation gap. This segment is different from the shallow decay segment (plateau) and flare, and may belong to a giant X-ray bump. We investigated this segment by the fall-back accretion model and found that the model can interpret this segment with reasonable parameter values. Within this physical model scenario, the fall-back accretion rate reaches a peak value $\sim 1.70 \times 10^{-5} M_{\odot}$ s^{-1} around 300 s in the central engine frame, which is compatible with the late mass supply rate of some low-metallicity massive progenitor stars. The initial black hole (BH) spin is $a_0 = 0.64^{+0.24}_{-0.26}$ and implies that this re-brightening signature requires a larger BH spin. The total accretion mass during the fall-back process is $M_{\rm acc} = (3.09 \pm 0.02) \times 10^{-2} M_{\odot}$. The jet energy from the fall-back accretion is $(9.77 \pm 0.65) \times 10^{52}$ erg, with a ratio of 0.066 to the isotropic-equivalent radiation energies of the GRB prompt phase in the 1–10^4 keV band. The fall-back radius r_p corresponding to the peak time of fall-back t_p is $(3.16 \pm 0.05) \times 10^{10}$ cm, which is consistent with the typical radius of Wolf–Rayet stars. In summary, our results provide additional support for the origin of the long burst from the core collapse of Wolf–Rayet stars, and its late central engine activity is likely due to the fall-back accretion process.

Key words: accretion – accretion disks – black hole physics – (stars:) gamma-ray burst: general

1. Introduction

Gamma ray bursts (GRBs) are the brightest electromagnetic event that have occurred in the universe since the Big Bang, consisting of two emission phases: the prompt emission(with an initial prompt soft γ-ray emission) and afterglow emission (with long term broadband emission). The prompt emission is generally considered to be related to the internal dissipation of the jet, such as internal shock dissipation or magnetic dissipation. Afterglow emission is usually considered to be from external shocks (especially forward shock) generated by the interaction between jets and interstellar medium (see Zhang 2018 for a review). In general, the end of the prompt emission phase means that the cease of GRB's central engine. However, observations from Swift satellite indicate that many GRB's central engines have an extended activity time, mainly manifested as shallow decay segments (plateaus) (Liang et al. 2007; Troja et al. 2007; Tang et al. 2019; Zhao et al. 2019), flares (Burrows et al. 2005; Zhang et al. 2006; Margutti et al. 2011), and giant bumps (Kumar et al. 2008a; Wu et al. 2013; Gao et al. 2016; Chen et al. 2017; Zhao et al. 2020, 2021) in the X-ray light curves following the prompt emission.

The Swift/XRT detected the X-ray afterglow of long burst GRB 220117A, which began to rebrighten 300 s after triggering and suggest that this GRB has an extended central engine activity time. In addition, this signature is different from X-ray shallow decay segment (plateau) and flare, and may belong to a giant X-ray bump. Due to the absence of an "internal plateau" feature in the X-ray afterglow of GRB 220117A, its central engine may be a hyperaccreting black hole (BH) system. In this physical scenario, the internal dissipation of fall-back accretion energy can interpret the giant X-ray bump. If the fall-back accretion rate or the duration of fall-back accretion process is large enough, a giant X-ray bump that rapidly rises and decays with a form of $t^{-5/3}$ is expected. So far, the giant X-ray bump has been found in the X-ray afterglow of many GRBs and could be well interpreted within the fall-back accretion model (Wu et al. 2013; Gao et al. 2016; Chen et al. 2017; Zhao et al. 2021).

In this paper, we study the X-ray re-brightening signature of GRB 220117A within the fall-back accretion model. In Section 2, we describe the observations of GRB 220117A and analyze the re-brightening signature. The fall-back accretion model is described in Section 3. In Section 4, we apply the fall-back accretion model to the re-brightening signature. The conclusion and implications of our results are discussed in Section 5. Throughout the paper, the convention $Q = 10^n Q_n$ is adopted in c.g.s. units.

2. GRB 220117A Observations

The BAT triggered and located GRB 220117A at 23:58:21 UT on 2022 January 17. T_{90}(15–350 keV) is 49.81 ± 2.37 s. The time-averaged spectrum from $T + 14.79$s to $T + 66.14$s is

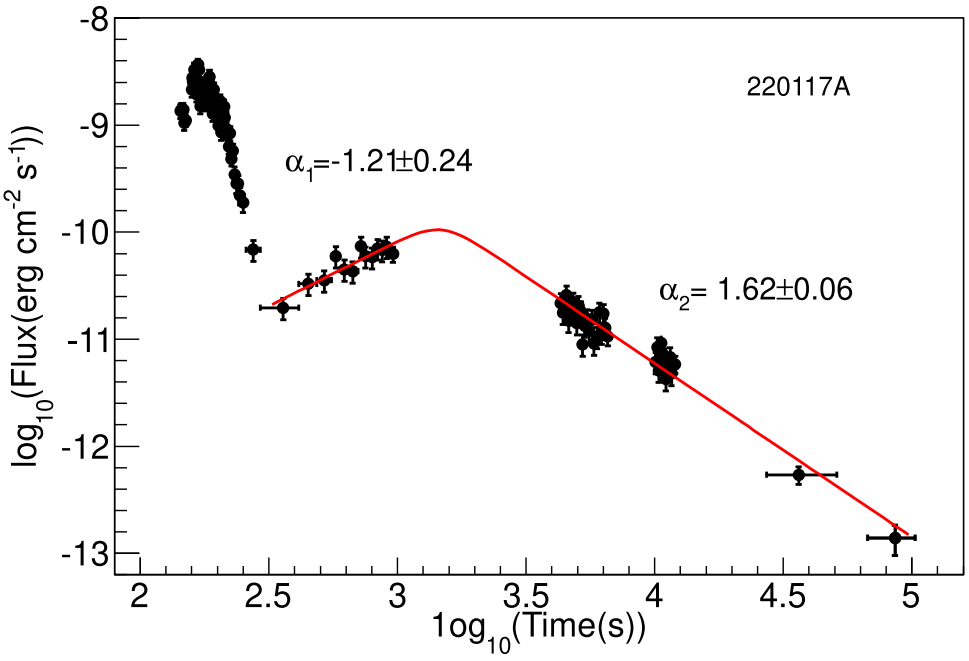

Figure 1. The XRT light curve of GTB 220117A. The solid red lines are the best fits with a smooth broken power law for the X-ray re-brightening phase and its follow-up decay phase.

best fitted by a single power law (SPL) function. The power-law index of the time-averaged spectrum is $\Gamma_\gamma = 1.8 \pm 0.18$. The fluence in the 15–150 keV band is $S_\gamma = 1.6 \pm 0.2 \times 10^{-6}$ erg cm^{-2}(Palmer et al. 2022). XRT observations started at 151.9 s after the trigger. The XRT light curve is shown in Figure 1. The UVOT starts collecting data 161 s after the trigger. No source was detected by the UVOT at the X-ray afterglow position (Melandri et al. 2022). Palmerio et al. (2022) observed the afterglow of GRB 220117A using the ESO VLT UT3. From the feature of Lyα trough and the Si II 1260 AA, the redshift was measured as $z = 4.961$.

For the re-brightening segment and follow-up segment of GRB 220117A, we adopted a smooth broken power law (BPL) function to fit it,

$$f(t) = f_0 \left[\left(\frac{t}{t_b} \right)^{w\alpha_1} + \left(\frac{t}{t_b} \right)^{w\alpha_2} \right]^{-1/s} \quad (1)$$

where α_1 and α_2 represent the decay scope before and after the break, respectively. w describes the sharpness of break, and here we adopt $w = 3$ as suggested by Liang et al. (2007). The fitting light curve and the best fitting parameters are shown in Figure 1. In 2019, Zhao et al. (2019) found that the decay scope of a shallow decay segment accords with normal distribution $\alpha_1 = 0.35 \pm 0.35$ based on 13 yr of Swift/XRT observation data. It can be inferred that X-ray re-brightening segment may not be a shallow decay segment.

In addition, we also tested whether the X-ray re-brightening segment and follow-up segment belong to the flare. Yi et al. (2016) analyzed the GRBs with significant flares observed by Swift/XRT from 2005 April to 2015 March and obtained an empirical relationship:

$$\log_{10} T_{\rm dur} = (-0.35 \pm 0.11) + (1.12 \pm 0.04) \times \log_{10}(T_{\rm peak}) \quad (2)$$

where $T_{\rm peak}$ is the peak time of the fare. $T_{\rm dur} = T_{\rm end} - T_{\rm start}$ is the duration of the flare, where $T_{\rm start}$ and $T_{\rm end}$ represent the start time and end time of the flare, respectively. $T_{\rm peak}$ and $T_{\rm dur}$ of each flare could be easily obtained by fitting the light curve with a smooth BPL function. We find that the duration of X-ray re-brightening segment and its follow-up decay segment deviates from the duration obtained by the empirical relationship 2σ. Compared to the typical flare, the giant X-ray bump has a relatively longer duration. Therefore, the X-ray re-brightening segment and follow-up segment may belong to a giant X-ray bump.

3. Model Description

In this paper, we intend to use the fall-back accretion model to interpret the X-ray re-brightening segment of GRB 220117A. The physical scenario of the fall-back accretion model is described as follows: the progenitor stars of long GRBs may be massive stars (Woosley 1993; Paczyński 1998; MacFadyen & Woosley 1999; Woosley & Bloom 2006), and

generally have a core-envelope structure. At the end of the massive stars' evolution, photodisintegration and electron capture will trigger core collapse and form a super accretion BH system. The relative jet is launched by the super accretion BH system through extracting the gravitational energy from the accreted material or the spin energy of the BH. When the relativistic jet successfully penetrates the envelope, it powers initial prompt emission and broadband afterglow emission of the GRB. During the process of jet penetration through the progenitor envelope, a part of jet energy is transferred to the envelope, which might help the supernova to explode. The bounding shock responsible for the associated supernova transfers kinetic energy to the envelope materials and a part of envelope materials would be ejected. The rest of envelope materials could fall back into around of BH and form an accretion disk (Kumar et al. 2008a, 2008b). The accretion disk may power a new relativistic jet through the neutrino-annihilations mechanism (Popham et al. 1999; Narayan et al. 2001; Di Matteo et al. 2002; Janiuk et al. 2004; Gu et al. 2006; Chen & Beloborodov 2007; Liu et al. 2007, 2015; Lei et al. 2009, 2017; Xie et al. 2016) or Blandford–Znajek (BZ) mechanism (Blandford & Znajek 1977; Lee et al. 2000; Li 2000; Lei et al. 2005, 2013). Compared with the neutrino-annihilations mechanism, the jet powered by the BZ mechanism will be cleaner and more powerful (Lei et al. 2017; Xie et al. 2017; Lloyd-Ronning et al. 2018). Therefore, the BZ mechanism is more likely to interpret the late central engine activity of long GRBs. A part of BZ energy would eventually be injected into the afterglow blast wave. If the injected energy is comparable to or even larger than the blast wave kinetic energy, it will generate some detectable signature such as a plateau in the X-ray afterglow (Zhao et al. 2020). In addition, the rest energy would undergo the internal dissipation process, which may generate the observed giant X-ray bump.

The evolution of the fall-back rate of progenitor envelope material can be described by a smooth BPL function as (Chevalier 1989; MacFadyen et al. 2001; Zhang et al. 2008; Dai & Liu 2012)

$$\dot{M}_{\rm fb} = \dot{M}_{\rm p}\left[\frac{1}{2}\left(\frac{t-t_0}{t_{\rm p}-t_0}\right)^{-s/2} + \frac{1}{2}\left(\frac{t-t_0}{t_{\rm p}-t_0}\right)^{5s/3}\right]^{-1/s}, \quad (3)$$

where t_0 is the starting time of the fall-back accretion in the central engine frame, $\dot{M}_{\rm p}$ is the peak of fall-back rate, and $t_{\rm p}$ is the peak time of fall-back rate in the central engine frame.

Progenitor envelope material falls back in the late time and forms an accretion disk, which will be viscous accretion by the BH. The accretion rate can be obtained as (Kumar et al. 2008a)

$$\dot{M} = \frac{M_d}{\tau_{\rm vis}}, \quad (4)$$

where $\tau_{\rm vis} \sim 1/\alpha\Omega_k$ is viscous timescale of accretion disk. α is a standard dimensionless viscosity parameter with values of $\sim$0.01–0.1, and Ω_k is the Kepler angular velocity of the accretion disk. Due to accretion disk mass M_d will increase with the fall-back from the envelope material and decrease with accretion. Therefore, (Kumar et al. 2008a; Lei et al. 2017)

$$\dot{M}_{\rm d} = \dot{M}_{\rm fb} - \dot{M}. \quad (5)$$

By combining Equations (4) and (5), the accretion rate can be obtained as

$$\dot{M} = \frac{1}{\tau_{\rm vis}} e^{-t/\tau_{\rm vis}} \int_{t_0}^{t} e^{t'/\tau_{\rm vis}} \dot{M}_{\rm fb} dt', \quad (6)$$

If the viscous timescale is larger than the accretion time, the BH will undergo a slow accretion process. The accretion rate of BH would be flat when $t > \tau_{\rm vis}$ and then begin to decrease with time, see Figure 7 in Lei et al. (2017). On the other hand, the BH will undergo rapid accretion process if $\tau_{\rm vis} \ll t$. The evolution of the accretion rate will follow the fall-back rate, i.e., $\dot{M} = \dot{M}_{\rm fb}$. In this paper, we assume that the accretion process of BH undergo a rapid accretion process.

The fall-back accretion can continuously extract the rotational energy of the BH through the BZ mechanism, and powers a Poynting dominated jet. A part of jet energy would undergo the internal dissipation process, which may generate the observed giant X-ray bump. To connect the observed X-ray luminosity L_X and BZ power $P_{\rm BZ}$, it is necessary to introduce efficiency factor η_X and jet beaming factor f_b

$$\eta_{\rm X} P_{\rm BZ} = f_b L_{\rm X}. \quad (7)$$

The power of the BZ mechanism to extract the rotational energy of BH can be written as (Lee et al. 2000; Li 2000; Wang et al. 2002; Lei et al. 2005, 2013, 2017; McKinney 2005; Lei & Zhang 2011; Chen et al. 2017; Liu et al. 2017; Lloyd-Ronning et al. 2018)

$$P_{\rm BZ} = 1.7 \times 10^{50} a_\bullet^2 m_\bullet^2 B_{\bullet,15}^2 f(a_\bullet) \ {\rm erg\ s^{-1}}, \quad (8)$$

with

$$f(a_\bullet) = 1 - \sqrt{\left(\frac{1+q}{2}\right)}, \qquad q = \sqrt{1-a_\bullet^2}, \quad (9)$$

where $a_\bullet$ is the dimensionless BH spin parameter, $m_\bullet = M_\bullet/M_\odot$ is the dimensionless BH mass, and $B_{\bullet,15}$ is strength of the magnetic field near the BH horizon in units of 10^{15} G. From the Equations (8) and (9), it can be seen that the BZ power mainly depends on parameters of $B_\bullet$, $m_\bullet$ and $a_\bullet$.

In general, the strength of the magnetic field near the BH horizon can be estimated by balancing the magnetic pressure on the BH horizon and ram pressure of the accretion flow at the inner edge of the accretion disk (Moderski et al. 1997)

$$\frac{B_\bullet^2}{8\pi} \approx \frac{\dot{M}c}{4\pi r_\bullet^2}, \quad (10)$$

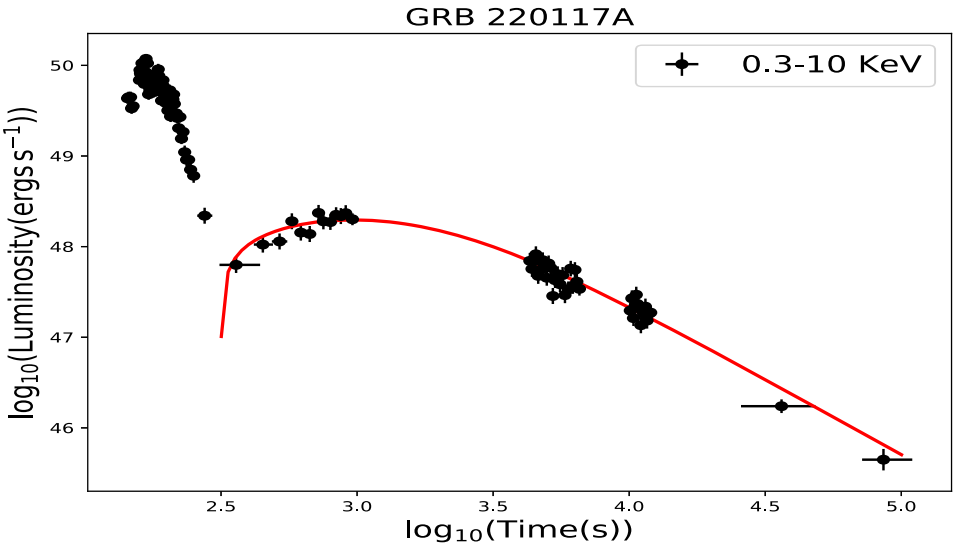

Figure 2. The fitting result of GRB 220117A's X-ray re-brightening segment by adopted the fall-back accretion model.

where $r_{\bullet} = (1 + \sqrt{1 - a_{\bullet}^2})GM_{\bullet}/c^2$ is radius of BH horizon.

The BZ process extracts rotational energy and angular momentum from the BH, while the accretion process brings the energy and angular momentum of the accretion disk into the BH. According to the conservation of energy and angular momentum, the evolution of BH under the two processes can be written as (Wang et al. 2002)

$$\frac{dM_{\bullet}c^2}{dt} = \dot{M}c^2E_{\rm ms} - P_{\rm BZ}, \tag{11}$$

$$\frac{dJ_{\bullet}}{dt} = L_{\rm ms}\dot{M} - T_{\rm BZ}. \tag{12}$$

From above two equations, it can be derived that

$$\frac{da_{\bullet}}{dt} = \frac{(\dot{M}L_{\rm ms} - T_{\rm BZ})c}{GM_{\bullet}^2} - \frac{2a_{\bullet}(\dot{M}c^2E_{\rm ms} - P_{\rm BZ})}{M_{\bullet}c^2}, \tag{13}$$

where $T_{\rm BZ}$ is the torque applied to the BH by the BZ process, which can be written as (Bardeen et al. 1972)

$$T_{\rm BZ} = 3.36 \times 10^{45}a_{\bullet}^2q^{-1}m_{\bullet}^3B_{\bullet,15}^2F(a_{\bullet})\,{\rm g\ cm^2\ s^{-2}}. \tag{14}$$

Here $E_{\rm ms}$ and $L_{\rm ms}$ are the specific energy and angular momentum at the radius of the innermost inner edge of accretion disk $R_{\rm isco}$, respectively, defined as (Novikov & Thorne 1973):

$$E_{\rm ms} = (4\sqrt{R_{\rm isco}} - 3a_{\bullet})/(\sqrt{3}R_{\rm isco}), \tag{15}$$

$$L_{\rm ms} = (GM_{\bullet}/c)(2(3\sqrt{R_{\rm isco}} - 2a_{\bullet}))/(\sqrt{3R_{\rm isco}}), \tag{16}$$

with

$$R_{\rm isco}(M_{\bullet}, a_{\bullet}) = \frac{GM_{\bullet}}{c^2}\{3 + z_2 - [(3 - z_1)(3 + z_1 + 2z_2)]^{1/2}\},$$
$$z_1 = 1 + (1 - a_{\bullet}^2)^{1/3}[(1 + a_{\bullet})^{1/3} + (1 - a_{\bullet})^{1/3}],$$
$$z_2 = (3a_{\bullet}^2 + z_1^2)^{1/2}. \tag{17}$$

4. Model Application to the X-Ray Re-brightening Signature of GRB 220117A

In this section, we apply the fall-back accretion model that was introduced in Section 3 to the X-ray re-brightening segment and follow-up segment of GRB 220117A. We adopt the start time of re-brightening segment $t_{\rm start} = t_{\rm start,obs}/(1+z)$ and the end time of follow-up segment $t_{\rm end} = t_{\rm end,obs}/(1+z)$ as the start time and the end time of the fall-back accretion in the central engine frame. According to analysis, the initial mass of BH hardly affects the BZ power. In this section, we adopt $M_{\bullet,0} = 3M_{\odot}$. In addition, we take $f_b = 0.01$ and $\eta_X = 0.01$ in our calculation. Finally, we take the dimensionless peak fall-back rate $\dot{m}_p$, the sharpness of the peak s, the peak time of fall-back rate t_p and initial BH spin a_0 as our free parameters. In order to obtain the best fitting values, a Markov Chain Monte Carlo (MCMC) method is adopted. In our MCMC fitting, the emcee code is used (Foreman-Mackey et al. 2013). In the code, we set the boundaries of four free parameters to $\log_{10}(\dot{m}_p) \equiv [-15, 0]$, $s \equiv [0, 10]$, $t_p \equiv [t_{\rm start}, t_{\rm end}]$ and $a_0 \equiv [0, 1]$, respectively.

The fitting result of GRB 220117A's X-ray re-brightening segment and follow-up segment is shown in Figure 2. In addition, Figure 3 shows the corner plot of the free parameters

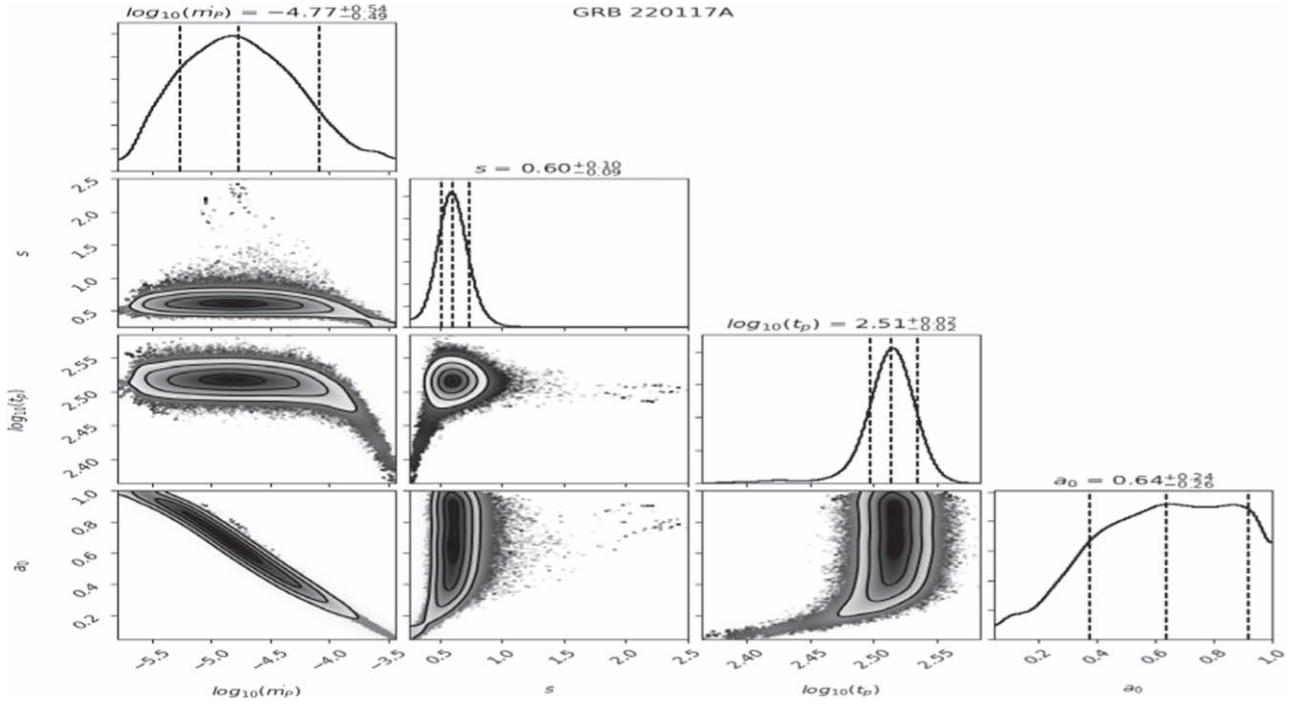

Figure 3. The corner plot of the free parameters posterior probability distribution for the fitting result.

posterior probability distribution. We adopt the median of the free parameter distribution and 1σ error as the fitting results, with the dimensionless peak fall-back rate is $\log_{10}(\dot{m}_p) = -4.77^{+0.54}_{-0.49}$, the sharpness of the peak is $s = 0.60^{+0.10}_{-0.09}$, the peak time of fall-back rate is $\log_{10}(t_p) = 2.51 \pm 0.02$ and the initial BH spin is $a_0 = 0.64^{+0.24}_{-0.26}$. From the fitting results, we calculated the total mass during the fall-back process is $M_{\rm acc} = (3.09 \pm 0.02) \times 10^{-2} M_{\odot}$, the strength of the magnetic field near the BH horizon at the t_p is $B_{p,15} = 0.089 \pm 0.0021$, the fall-back radius corresponding to t_p is $r_p = (3.16 \pm 0.05) \times 10^{10}$cm and the jet energy from the fall-back accretion is $(9.77 \pm 0.65) \times 10^{52}$erg, with a ratio of 0.066 to the isotropic-equivalent radiation energies of the GRB prompt phase in the 1–10^4 keV band.

In conclusion, the fall-back accretion model can interpret the X-ray re-brightening segment and follow-up segment with reasonable parameter values. This signature may require a larger black hole spin (the peak of its posterior probability distribution is $a_0 = 0.64^{+0.24}_{-0.26}$). When the fall-back rate reaches its peak, the corresponding fall-back radius is consistent with the typical radius of a Wolf Rayet star. This result provides further support for the origin of the long GRB from the core collapse of the Wolf–Rayet stars, and its late central engine activity is likely due to the fall-back accretion process.

The fallback accretion rate reaches a peak value $\sim 1.70 \times 10^{-5} M_{\odot}\,{\rm s}^{-1}$ around 300 s in the central engine frame. The bounding shock responsible for the associated supernova transfers kinetic energy to the envelope materials and most of the envelope materials would be ejected. Therefore, it is very necessary to check whether the progenitor of GRB 220117A can provide enough envelope material. The fall-back rate of envelope material can be estimated by the data of pre-SN models, i.e., (Suwa & Ioka 2011; Woosley & Heger 2012; Matsumoto et al. 2015; Liu et al. 2018)

$$\dot{M}_{\rm fb} = \frac{2M_r}{t_{\rm ff}}\left(\frac{\rho}{\bar{\rho} - \rho}\right), \tag{18}$$

where $\bar{\rho}$ is the average density within radius r, $t_{\rm ff}$ is the freefall timescale of envelope material with radius r. It can be obtained as

$$t_{\rm ff}(r) = \frac{\pi}{2}\sqrt{\frac{r^3}{2GM_{\rm r}}} \tag{19}$$

where M_r is the mass within the radius r. The value can be obtained by the following equation

$$M_r = M_{\bullet,0} + \int_{r_0}^{r} 4\pi r^2 \rho dr, \tag{20}$$

where ρ is the density of envelope material at radius r. We set the time and radial coordinate for which the enclosed mass reach initial black hole mass as r_0 and 0, respectively. By adopt the progenitor density profile with different metallicities and masses from Liu et al. (2018), we calculate evolution of the mass supply rate for theirs and are shown in Figure 4. We find

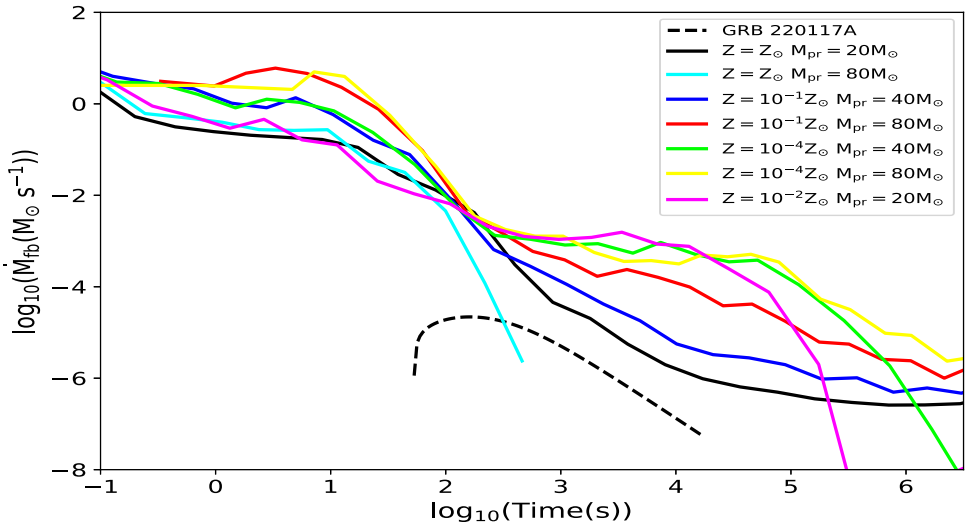

Figure 4. The evolution of the mass supply rate of progenitor with different metallicities and masses. The dashed line represents fall-back rate evolution of GRB 220117A's progenitor envelope material in our fitting. $Z_{\odot}$ is the metallicities of the Sun.

that low-metallicity massive progenitor stars are compatible with our fitting results.

5. Discussion and Conclusions

The Swift/XRT detected the X-ray afterglow of long burst GRB 220117A, which began to rebrighten 300 s after triggering and followed a single power-law decay segment after thousands of seconds of the orbital observation gap. The re-brightening segment is different from the shallow decay segment (plateau) and flare, and may belong to a giant X-ray bump. We investigated this segment by the fall-back accretion energy internal dissipation model. We found that the model can interpret this segment with reasonable parameter values. Within this physical model scenario, the fallback accretion rate reaches a peak value $\sim 1.70 \times 10^{-5} M_{\odot}\,\mathrm{s}^{-1}$ around 300 s in the central engine frame, which is compatible with the late mass supply rate of some low-metallicity massive progenitor stars. The initial BH spin is $a_0 = 0.64^{+0.24}_{-0.26}$ and implies that this re-brightening signature requires a larger BH spin. The total accretion mass $M_{\rm acc}$ during the fall-back process is $M_{\rm acc} = 3.09 \times 10^{-2} M_{\odot}$. The jet energy from the fall-back accretion is $(9.77 \pm 0.65) \times 10^{52}$erg, with a ratio of 0.066 to the isotropic-equivalent radiation energies of GRB prompt phase in the $1–10^4$ keV band. The fall-back radius r_p corresponding to t_p is $(3.16 \pm 0.05) \times 10^{10}$cm, which is consistent with the typical radius of Wolf–Rayet stars. In summary, our results provide additional support for the origin of the long burst from the core collapse of Wolf–Rayet stars, and its late central engine activity is likely due to the fall-back accretion process.

In this paper, we adopted a simple fall-back accretion rate evolution model, and do not consider the angular momentum distribution of the progenitor star, so this calculation is approximately valid for a slowly rotating progenitor. In fact, the angular velocities Ω of stars with different radii are different and the fall-back radius satisfies $\propto \Omega^2$ (Kumar et al. 2008a). Therefore, the angular momentum distribution of the progenitor star has a great influence on the fall-back accretion rate. In addition, the metallicities and masses of stars will have a certain impact on the fall-back accretion rate of the envelope material. In the future, we will study the fall-back accretion model with different angular momentum distribution, mass distribution and metallicity.

Super Eddington accretion makes material on the accretion disk subject to an outward radiation pressure that is greater than gravity, Therefore, an outflow (i.e., disk wind) driven by radiation pressure is launched on the surface of the accretion disk, and taking away a part of the fall-back materials. However, the disk wind is ignored in the fall-back accretion model adopted in this paper. It will cause the accretion rate of BH to decrease. Because the outflow of the accretion disk is not well understood, the power law function model is generally adopted to describe the accretion rate at different accretion disk radii. It can be seen that the influence from the outflow of the accretion disk to the accretion rate is highly dependent on the power law index. In addition, the existence of the accretion disk outflow will also be important for understanding the baryon load of a GRB jet (Lei et al. 2013, 2017) and ^{56}Ni synthesis for associated supernovae (Song & Liu 2019). We hope that the future general-relativistic magnetohydrodynamic (GRMHD) simulations can help us better understand the accretion disk outflow.

References

Bardeen, J. M., Press, W. H., & Teukolsky, S. A. 1972, ApJ, 178, 347
Blandford, R. D., & Znajek, R. L. 1977, MNRAS, 179, 433
Burrows, D. N., Romano, P., Falcone, A., et al. 2005, Sci, 309, 1833
Chen, W., Xie, W., Lei, W.-H., et al. 2017, ApJ, 849, 119
Chen, W.-X., & Beloborodov, A. M. 2007, ApJ, 657, 383
Chevalier, R. A. 1989, ApJ, 346, 847
Dai, Z. G., & Liu, R.-Y. 2012, ApJ, 759, 58
Di Matteo, T., Perna, R., & Narayan, R. 2002, ApJ, 579, 706
Foreman-Mackey, D., Hogg, D. W., Lang, D., & Goodman, J. 2013, PASP, 125, 306
Gao, H., Lei, W.-H., You, Z.-Q., et al. 2016, ApJ, 826, 141
Gu, W.-M., Liu, T., & Lu, J.-F. 2006, ApJL, 643, L87
Janiuk, A., Perna, R., Di Matteo, T., et al. 2004, MNRAS, 355, 950
Kumar, P., Narayan, R., & Johnson, J. L. 2008a, MNRAS, 388, 1729
Kumar, P., Narayan, R., & Johnson, J. L. 2008b, Sci, 321, 376
Lee, H. K., Wijers, R. A. M. J., & Brown, G. E. 2000, PhR, 325, 83
Lei, W.-H., Wang, D.-X., & Ma, R.-Y. 2005, ApJ, 619, 420
Lei, W. H., Wang, D. X., Zhang, L., et al. 2009, ApJ, 700, 1970
Lei, W.-H., & Zhang, B. 2011, ApJL, 740, L27
Lei, W.-H., Zhang, B., & Liang, E.-W. 2013, ApJ, 765, 125
Lei, W.-H., Zhang, B., Wu, X.-F., & Liang, E.-W. 2017, ApJ, 849, 47
Li, L.-X. 2000, PhRvD, 61, 084016
Liang, E.-W., Zhang, B.-B., & Zhang, B. 2007, ApJ, 670, 565
Liu, T., Gu, W.-M., Xue, L., et al. 2007, ApJ, 661, 1025
Liu, T., Gu, W.-M., & Zhang, B. 2017, NewAR, 79, 1
Liu, T., Hou, S.-J., Xue, L., et al. 2015, ApJS, 218, 12
Liu, T., Song, C.-Y., Zhang, B., Gu, W.-M., & Herger, A. 2018, ApJ, 852, 20
Lloyd-Ronning, N. M., Lei, W.-H., & Xie, W. 2018, MNRAS, 478, 3525
MacFadyen, A. I., & Woosley, S. E. 1999, ApJ, 524, 262
MacFadyen, A. I., Woosley, S. E., & Heger, A. 2001, ApJ, 550, 410
Margutti, R., Bernardini, G., Barniol Duran, R., et al. 2011, MNRAS, 410, 1064
Matsumoto, T., Nakauchi, D., Ioka, K., et al. 2015, ApJ, 810, 64
McKinney, J. C. 2005, ApJL, 630, L5
Melandri, A., Bernardini, M. G., D'Avanzo, P., et al. 2022, GRB Coordinates Network, Circular Service, No. 31466, 31466
Moderski, R., Sikora, M., & Lasota, J. P. 1997, Relativistic Jets in Agns in Proc. Int. Conf., (Cracow: The Editors), 110
Narayan, R., Piran, T., & Kumar, P. 2001, ApJ, 557, 949
Novikov, I. D., & Thorne, K. S. 1973, Black Holes (Les Astres Occlus), Vol. 343 (New York: Gordon and Breach)
Paczyński, B. 1998, ApJL, 494, L45
Palmer, D. M., Barthelmy, S. D., Krimm, H. A., et al. 2022, GRB Coordinates Network, Circular Service, No. 31485, 31485
Palmerio, J., Malesani, D. B., Fynbo, J. P. U., et al. 2022, GRB Coordinates Network, Circular Service, No. 31480, 31480
Popham, R., Woosley, S. E., & Fryer, C. 1999, ApJ, 518, 356
Song, C.-Y., & Liu, T. 2019, ApJ, 871, 117
Suwa, Y., & Ioka, K. 2011, ApJ, 726, 107
Tang, C.-H., Huang, Y.-F., Geng, J.-J., et al. 2019, ApJS, 245, 1
Troja, E., Cusumano, G., O'Brien, P. T., et al. 2007, ApJ, 665, 599
Wang, D. X., Xiao, K., & Lei, W. H. 2002, MNRAS, 335, 655
Woosley, S. E. 1993, ApJ, 405, 273
Woosley, S. E., & Bloom, J. S. 2006, ARA&A, 44, 507
Woosley, S. E., & Heger, A. 2012, ApJ, 752, 32
Wu, X.-F., Hou, S.-J., & Lei, W.-H. 2013, ApJL, 767, L36
Xie, W., Lei, W.-H., & Wang, D.-X. 2016, ApJ, 833, 129
Xie, W., Lei, W.-H., & Wang, D.-X. 2017, ApJ, 838, 143
Yi, S.-X., Xi, S.-Q., Yu, H., et al. 2016, ApJS, 224, 20
Zhang, B. 2018, The Physics of Gamma-Ray Bursts (Cambridge: Cambridge Univ. Press)
Zhang, B., Fan, Y. Z., Dyks, J., et al. 2006, ApJ, 642, 354
Zhang, W., Woosley, S. E., & Heger, A. 2008, ApJ, 679, 639
Zhao, L., Gao, H., Lei, W., et al. 2021, ApJ, 906, 60
Zhao, L., Liu, L., Gao, H., et al. 2020, ApJ, 896, 42
Zhao, L., Zhang, B., Gao, H., et al. 2019, ApJ, 883, 9